Spectrochimica Acta Part B: Atomic Spectroscopy 193 (2022) 106435

Contents lists available at ScienceDirect

Spectrochimica Acta Part B: Atomic Spectroscopy

journal homepage: www.elsevier.com/locate/sab

Laser-induced breakdown spectroscopy signal enhancement effect for argon caused by the presence of gold nanoparticles

Dávid J. Palásti [a,b], Lajos P. Villy [b,c], Attila Kohut [b,c], Tibor Ajtai [c], Zsolt Geretovszky [b,c], Gábor Galbács [a,b,d,*]

[a] Department of Inorganic and Analytical Chemistry, University of Szeged, 6720 Szeged, Dóm sq. 7, Hungary
[b] Department of Materials Science, Interdisciplinary Excellence Centre, University of Szeged, 6720 Szeged, Dugonics sq. 13., Hungary
[c] Department of Optics and Quantum Electronics, University of Szeged, 6720 Szeged, Dóm sq. 9, Hungary
[d] Department of Applied and Nonlinear Optics, Institute for Solid State Physics and Optics, Wigner Research Centre for Physics, Konkoly-Thege M. Way 29-33, 1121 Budapest, Hungary

ARTICLE INFO

Keywords:
Nanoparticle-enhanced LIBS (NELIBS)
Electrical discharge nanoparticle generator
Signal enhancement
Indirect nanoparticle detection
Trace gas analysis

ABSTRACT

The effect of the presence of nanoparticles (NPs) on the laser induced breakdown spectroscopy (LIBS) signal of argon gas was studied experimentally. 10–20 nm diameter gold NPs, produced by a spark discharge nanoparticle generator, were suspended in argon gas. The effect of particle size, number concentration and mass concentration, as well as laser pulse energy on the LIBS argon signal was systematically investigated. It was found that the breakdown threshold of the gas decreases considerably, facilitating the detection of Ar emission at such laser fluences, which do not allow plasma formation without the presence of the NPs. Our observations persist even at aerosol mass concentrations that are too low to allow the direct detection of nanoparticles. The effect, which is attributed to electron thermo- and field emission induced by the high intensity laser pulse, shows an asymptotically increasing magnitude with the aerosol mass concentration. The signal enhancement was found to be 10^2–10^4 and the effect is suggested to be useful in trace gas analysis or for the indirect detection of NPs. The achievable indirect aerosol mass concentration detection limit was estimated to be in the parts per trillion regime (as low as 50 ng·m^{-3}), which is comparable to the best literature values reported for direct analysis.

1. Introduction

Laser-induced breakdown of gases has been observed decades ago to be facilitated by the presence of fine (micrometer-sized) liquid or solid particles suspended in the gas. It was documented by several studies that in the presence of particles, the breakdown threshold of gases decreased by up to the order of one hundred [1,2]. This effect was mainly attributed to focusing (amplification of electrical field strength) and the local heating of the particle surface (leading to thermoelectric emission) [3]. It has been established that the mechanisms behind the effect depend on the particle size, refractive index and absorption at the laser wavelength. For transparent particles (e.g. liquid droplets) an additional localized geometrical focusing of the laser beam also occurs. It was also found that aqueous aerosols do not reduce the threshold as much as solid aerosols [4], but the pressure [5], wavelength [6] and material-related aspects [7] of the effect for droplets were explored. It was also a subject of investigation whether the breakdown occurs outside or inside the aerosol particle [2]. The topic of the breakdown induced by micrometer-sized aerosol particles was reviewed e.g. by Budnik and Zakharchenko [8] and Raizer [9]. The effect of nanoparticles on the laser-induced breakdown of gases however has not been investigated yet.

A different, but related LIBS application is aerosol characterization, which is actually quite appealing in various fields, such as industrial process monitoring or atmospheric environmental studies, due to that robust and remotely operated analytical techniques capable of providing real-time, in situ qualitative and quantitative analytical information about aerosol particles are very rare. As a consequence of this, LIBS aerosol analysis was explored as early as in the 1980's [10] and the field has considerably expanded over the decades, as it is reflected in the number of reviews and book chapters dedicated to the topic (e.g. [11–14]). The size-resolved analysis of micron and sub-micron sized aerosols, as well as on-line (free-stream, e.g. [15,16]) and off-line (following collection on filters, e.g. [17,18]) sampling approaches were equally reported. Important contributions to the field were made

* Corresponding author at: Department of Inorganic and Analytical Chemistry, University of Szeged, 6720 Szeged, Dóm sq. 7, Hungary.
E-mail address: galbx@chem.u-szeged.hu (G. Galbács).

https://doi.org/10.1016/j.sab.2022.106435
Received 12 February 2022; Received in revised form 25 April 2022; Accepted 26 April 2022
Available online 30 April 2022

by Hahn and co-workers, e.g. with respect to sampling statistics, triggering, assessing the upper size limitation on the complete ablation of particles, distinguishing between gaseous and particulate phase analytes, and other aspects (e.g. [11,13–15]).

Investigations in the LIBS literature that successfully attempted the detection of aerosol nanoparticles (NPs) directly are quite scarce [19]. For example, Amodeo et al. performed monitoring of silicon carbide NPs synthesized by laser pyrolysis in the size range of 20 to 100 nm [16]. Strauss et al. reported size-resolved composition-related measurements of calcium chloride NPs (20 to 800 nm) [20]. Purohit, Fortes et al. demonstrated the feasibility of the individual detection and characterization of several metal and metal oxide NPs by their proprietary *optical catapulting-optical trapping* method (e.g. [21,22]). Zhang et al. introduced the methodology of *low-intensity phase-selective LIBS*, and successfully exploited it for the detection of TiO_2 aerosol NPs sometimes as small as 6 nm in diameter [23]. Optical trapping or "preconcentration and release" [24] approaches avoid the problem of ultra-low sampling rates with direct LIBS aerosol analysis, and allow for bringing the mass detection limit down to the ng·m^{-3} range (or to the attogram regime in absolute terms) from the typical μg·m^{-3} range.

In the present project, we focused on how the presence of 10–20 nm diameter gold nanoparticles affect the LIBS signal of argon gas in which the nanoparticles are suspended. We studied the effect of particle size and particle number concentration on the argon gas LIBS signal enhancement, as well as their influence on the breakdown threshold. As a nanoparticle source, we used the output from a spark discharge nanoparticle generator (SDG) which produces the particles already suspended in a gas. In recent years, these innovative nanoparticle generators have become commercially available in a compact form (see e.g. the GFG series from Palas (Germany), the APG series from Sibata Technology (Japan), the VSP-G1 from VSParticle (The Netherlands), etc.) and are getting known for their productivity, energy efficiency, versatility and particle purity [25–29]. At the same time, they are also good model sources, as the particle properties (size distribution, concentration and composition) can be relatively easily controlled [30,31].

2. Experimental

2.1. Instrumentation

The central part of the spark discharge generator system used here for the generation of gold nanoparticles is a vacuum chamber, in which the applied cylindrical, gold electrode pair was horizontally positioned and axially aligned with a 2.0 mm gap left between them (spark gap). The gap size was controlled by micro-positioners (Model K150-BLM-1, MDC Vacuum Ltd.). The 5.0 standard liter per minute (slm) argon carrier gas flow, controlled by a mass flow controller (Model GFC16, Aalborg Inc.), was fed in the chamber via the bottom port of the chamber (upward pointing "crossflow" with injector nozzle) [31]. All experiments were carried out at near atmospheric pressure (controlled at 1100 mbar). An 8 nF, monolithic, high voltage, pulse discharge capacitor (Model 450 PM980, General Atomics) was connected to the spark gap and charged by a high voltage capacitor charging power supply (Model HCK 800-12500, FuG GmbH). The discharge of the capacitor between the electrodes commences when the voltage on the capacitor reaches the breakdown voltage in the electrode gap. The resulting spark discharge is a bipolar, oscillatory discharge. The repetition rate of the sparking, which affects the size distribution and number concentration of the generated aerosol, can be adjusted by controlling the charging current of the capacitor. The created gold NPs were lead through a 900°C compaction tube furnace (EHA 12/300B, Carbolite Gero GmbH), so the attached primary particles were sintered together. The concentration of the particles was controlled by commercial (VKL 10, Palas GmbH) and/or in house-built dilution systems. The size distribution of the spark generated particles was measured using a scanning mobility particle sizer (SMPS) system consisting of an electrostatic classifier (3082, TSI), an ultrafine condensation particle counter (3756, TSI), and an aerosol charge neutralizer (Kr-85, NRD). A schematic of the experimental setup is illustrated in Fig. 1. The size distribution of the produced gold nanoparticles used in the particle size dependency experiments (with 10 and 18 nm modi) are shown in Fig. 2.

LIBS experiments were carried out in a flow-through, small volume ablation chamber constructed for LIBS aerosol measurements and described in detail elsewhere [32]. The Nd:YAG laser (Quantel Ultra 100, Lumibird) emitted 10 ns long pulses at the fundamental 1064 nm wavelength. The pulse energy delivered was varied between 30 and 90 mJ. The beam was focused into the chamber from above through a 1 mm thick UV-grade fused silica window using an AR-coated high-power laser focusing objective (LMH-5×-1064, Thorlabs Inc.). The laser fluence was 6 to 18·10^2 J·cm^{-2} for the pulse energy range used. The repetition rate of the laser was set to a low value (ca. 1 Hz) to ensure that the argon flow fully purges the chamber between laser shots. Each experiment was carried out with one hundred laser pulses in a batch and in three repetitions. The LIBS plasma was observed via two fused silica collimating lenses implemented in two ports located on the sides of the chamber (collecting light from the same spot in the chamber in the horizontal direction, with a 90° angle between the optical axes of the two lenses). The collected light was coupled into a two-channel fiber-optic CCD spectrometer (AvaSpec-FT2048, Avantes) using solarization-resistant, 200 μm core diameter, 0.22 NA optical fibers (FCB-UV200-2-SR, Avantes). The measurement chamber was mounted on a translation stage, which allowed bringing the laser focal spot inside the chamber in front of the light collection lenses. Gating of the spectral data collection was achieved by the internal electronics of the spectrometer, which was triggered by the laser power supply unit and continuously monitored on a digital storage oscilloscope (TDS1002, Tektronix). The minimum possible gate delay of 1 μs and gate width of 2 ms was set at the spectrometer. The spectrometer allowed the recording of the plasma emission in the 198–318 nm (UV) and 344–888 nm (Vis) spectral ranges, with optical resolutions of 0.09 nm and 0.4 nm, respectively.

2.2. Materials

The cylindrical gold electrodes of 99.9% purity and 3.0 mm in diameter were obtained from Goodfellow Cambridge Ltd. (UK). Argon gas of 99.996% purity (Messer Hungarogáz Ltd.) was employed as carrier and dilution gas.

2.3. Data evaluation

All spectra were recorded using the AvaSoft 7.2 program (Avantes). The data import and background correction were achieved using an R script (R 4.1.2, cran.r-project.org), while data evaluation and graphing was carried out using MS Office Excel 2016 (Microsoft) and Origin 2018 Pro (OriginLab) software. Spectral line assignation was done using the online NIST Atomic spectra database.

Since not all laser pulses delivered into the nanoaerosol resulted in the formation of an argon breakdown plasma, we defined two quantities (objective variables) for the description and discussion of the observations. A plasma was considered to be formed if significant plasma emission from the carrier gas could be detected at the Ar I 794.8 nm line. This was established numerically by checking if the net intensity of the Ar spectral line increased with at least three times the standard deviation at the same wavelength, compared to the case when no aerosol particles were present. The *frequency of plasma formation* was expressed in percentages, relative to the delivered laser pulses. The quantity of *mean effective intensity* was calculated as the mean of the net intensity of the Ar I 794.8 nm indicator line based on instances in which a plasma was formed.

Excitation temperature of the Ar I species was calculated via the well-known Boltzmann plot method [33] by using a purpose-made Python code. Selected spectral lines used for the calculations with their

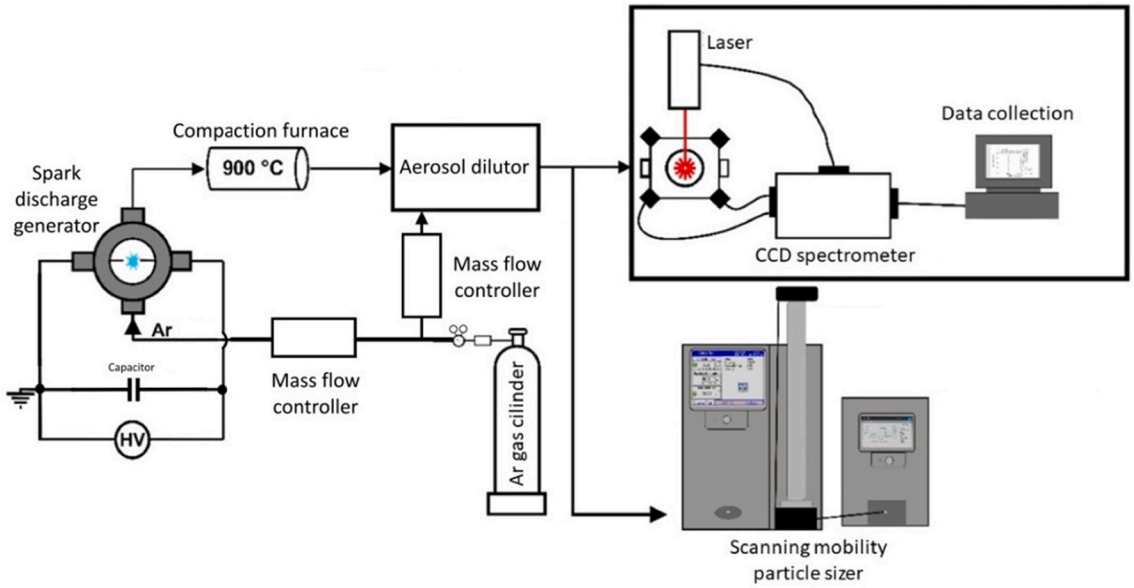

Fig. 1. Schematic illustration of the experimental setup.

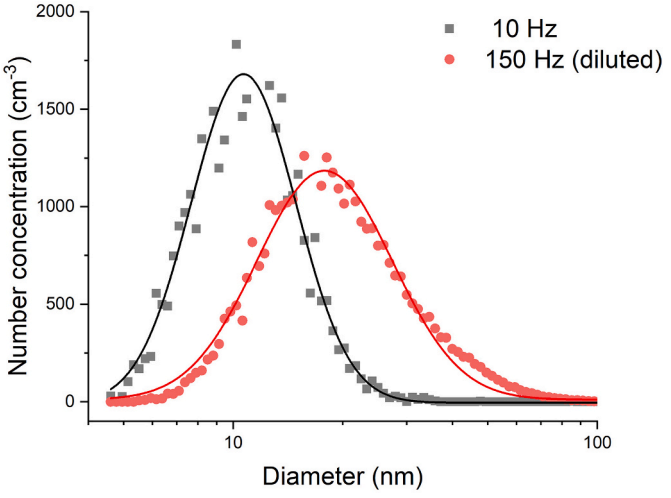

Fig. 2. Size distribution of the gold nanoaerosols generated by the SDG, using a 2 mm electrode gap, 5 slm Ar flow and 1.1 Ω circuit resistance, with the indicated spark repetition rates. (For interpretation of the references to colour in this figure legend, the reader is referred to the web version of this article.)

Table 1
Data of selected Ar transitions used in the Boltzmann temperature determination. λ_{ij} is the emission wavelength, E_i and g_i are the energy and the statistical weight of the upper level, respectively. A_{ij} is the transition probability.

Line	λ_{ij} [nm]	E_i [cm^{-1}]	g_i	A_{ij} [$\times 10^7$ s^{-1}]
Ar I	675.28	118,907	5	0.193
Ar I	687.13	118,651	3	0.278
Ar I	750.39	108,723	1	4.5
Ar I	794.82	107,132	3	1.86
Ar I	826.45	107,496	3	1.53
Ar I	852.14	107,132	3	1.39

respective atomic data are tabulated in Table 1. All constants are taken from the NIST database [34].

3. Results

The initial observation was that the gas breakdown was only detectable if gold NPs were suspended in the gas, even at very low concentrations. In the absence of the nanoparticles, there was no plasma emission. At the same time, in cases when there was plasma emission, the LIBS spectrum only contained argon lines; no emission from gold could be detected. This latter observation indicated that the mass concentration of gold in the aerosol is too low for detection. When nanoparticles were present in the gas the intensity of the indicator argon line fluctuated greatly, showing a high variance (random character). These findings, which lead us to perform a systematic study of the influence of the experimental parameters, are illustrated in Fig. 3.

3.1. Effect of particle concentration and laser pulse energy

In the first series of experiments, we investigated the influence of the particle number concentration and laser pulse energy on the objective variables (plasma formation frequency and mean effective intensity). The number concentration was varied between $1.4{\cdot}10^5$ and $2.8{\cdot}10^6$ cm^{-3} by aerosol dilution, whereas the laser pulse energy was varied between 30 and 90 mJ, in 5 mJ increments. The mode of the Au NP size distribution was 15 nm throughout the experiments. Both of the experimental parameters were found to have a strong, interrelated influence on the objective variables, which is illustrated in the graphs of Fig. 4.

As can be seen, both objective variables have a positive correlation with both experimental parameters meaning that all curves are monotonously increasing with the increase of the experimental parameters. All plots are non-linear. It is clearly the plasma formation frequency variable which has the stronger dependency on the experimental parameters; a change with a factor of a few changes the plasma formation frequency with ca. two orders of magnitude. In fact, the plasma formation frequency quickly reaches 100% at medium pulse energy and concentration values. At the same time, the effective signal intensity has a weaker dependency on the experimental parameters, especially on the concentration; a ca. an order of magnitude change in the concentration only produces a factor of 4–6 change in the intensity.

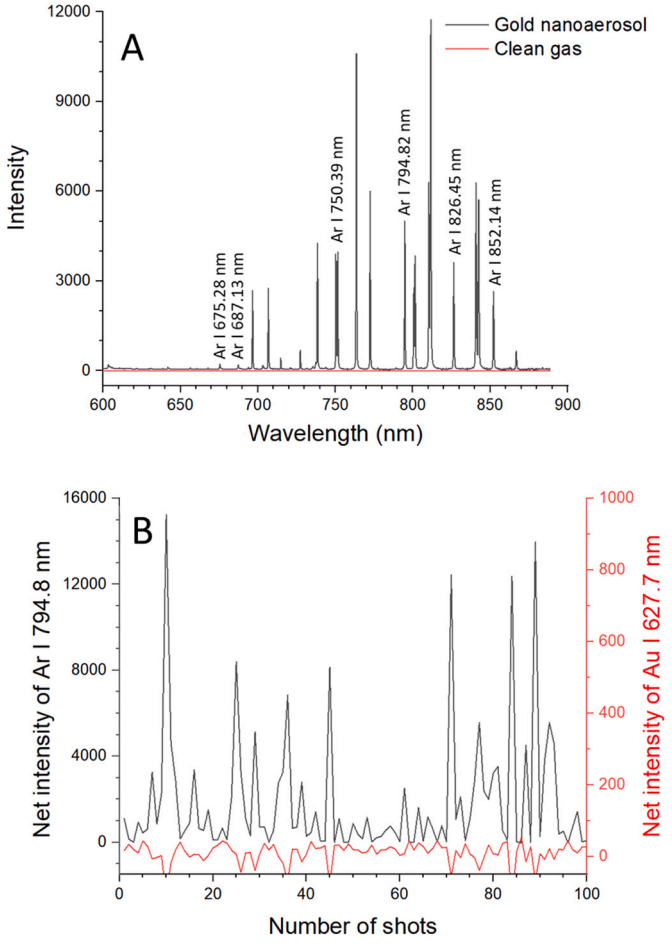

Fig. 3. The recorded emission spectrum with and without nanoparticles (upper panel), and the variation of the spectral intensity for argon and gold as a function of laser pulses delivered into the flowing aerosol (bottom panel). Conditions: 50 mJ pulse energy, $1.4{\cdot}10^6$ cm^{-3} concentration of Au NPs with a modal diameter of 15 nm. (For interpretation of the references to colour in this figure legend, the reader is referred to the web version of this article.)

3.2. Effect of particle size

As the size of NPs usually have a profound effect on their properties, we also studied its influence on the argon LIBS signal. For this study, the LIBS experiments were performed on two ensembles of Au NPs that had significantly different size (the mode of their size distribution was 10 nm and 18 nm), the laser pulse energy was set to 50, 60 and 80 mJ. The shift of the particle size distribution was achieved by tuning the SDG operating conditions (primarily the spark repetition rate [30,31]). The particle number concentration was kept as constant as possible, at a value between 3.6 and $3.8{\cdot}10^5$ cm^{-3}, via aerosol dilution.

As it can be seen in the set of graphs in Fig. 5, the value of the objective variables increases significantly with the increasing NP size. If there is plasma formation, then the effective mean intensity is roughly proportional to the cube of the change of particle size, suggesting a proportionality with the volume (or mass) of the particles. Somewhat surprisingly, the frequency of plasma formation also substantially increased along with the particle size, and its effect varied with the pulse energy as well. At 50 mJ, the 10 nm NPs were too small to create a plasma, while at 80 mJ they were able to ignite the gas plasma, but with a ca. 40% less frequency compared to the case of bigger particles. This also suggests that the effect increases with the particle size.

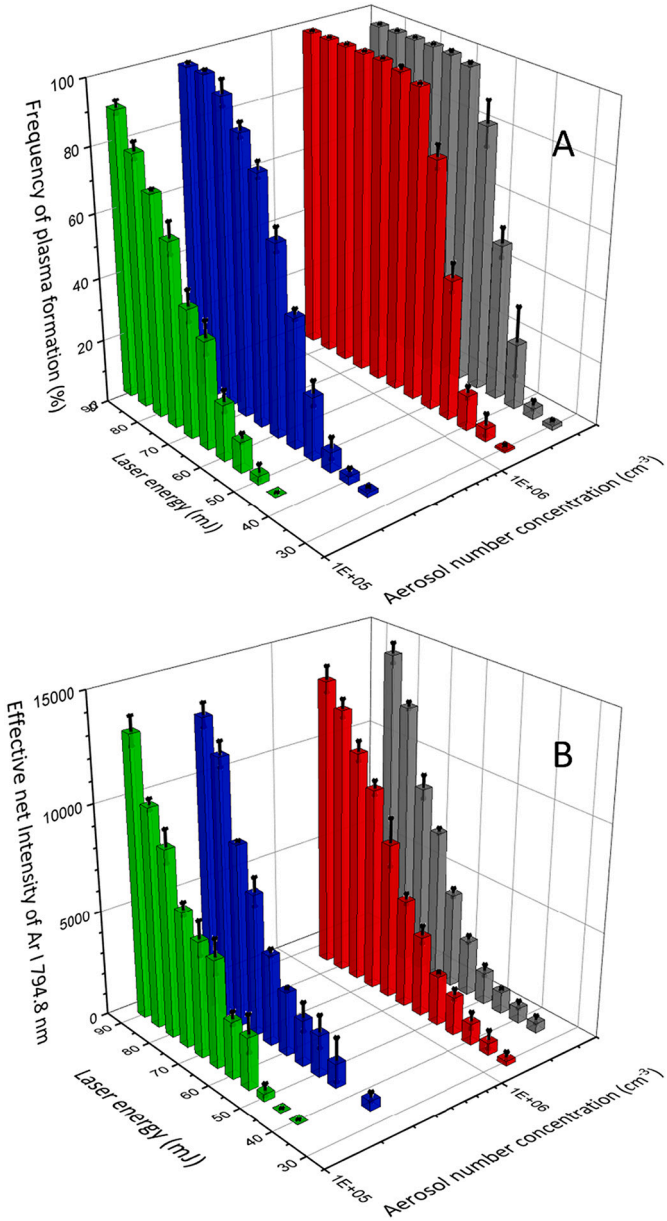

Fig. 4. Effect of the laser pulse energy and gold NP concentration on the plasma formation frequency (A) and the effective mean argon intensity (B). The modal diameter of Au NPs was 15 nm. All values shown are based on the mean of three replicate measurements, each based on data from 100 laser shots. (For interpretation of the references to colour in this figure legend, the reader is referred to the web version of this article.)

3.3. Effect of aerosol mass concentration

Based on our observation that both the particle size and concentration have a positive correlation with the argon signal enhancement (and plasma formation frequency), considering that the effective intensity seems to have a cubic relation with the particle diameter, it is plausible to assume that the argon signal is a function of the aerosol mass concentration. In order to clarify this assumption, we repeated the experiments at four pulse energy values (40, 50, 60 and 80 mJ) with varying the aerosol mass concentration in a range over three orders of magnitude. The concentration range was achieved by tuning the SDG operating parameters combined with aerosol dilution. Under all conditions, the actual modal particle size and concentration was monitored by a scanning mobility particle sizer.

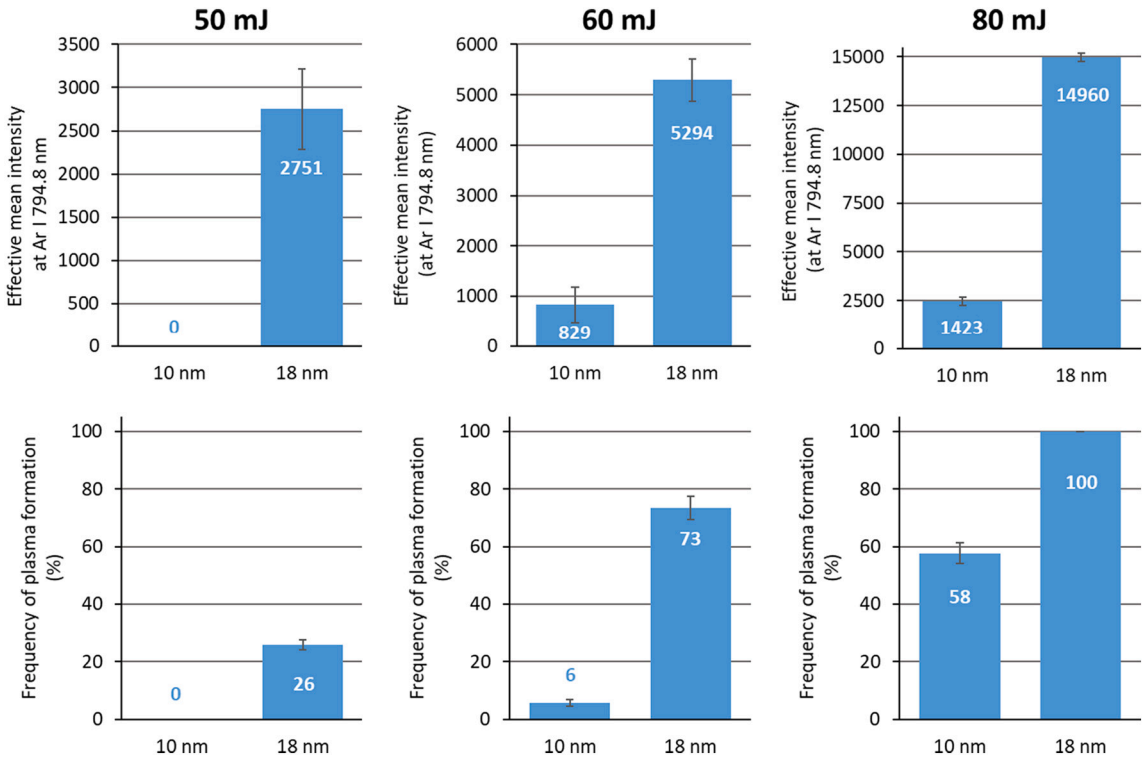

Fig. 5. Effect of the modus of the size distribution of gold NPs on the two objective variables. All values shown are based on the mean of three replicate measurements, each based on data from 100 laser shots. Errors bars indicate the standard deviation. (For interpretation of the references to colour in this figure legend, the reader is referred to the web version of this article.)

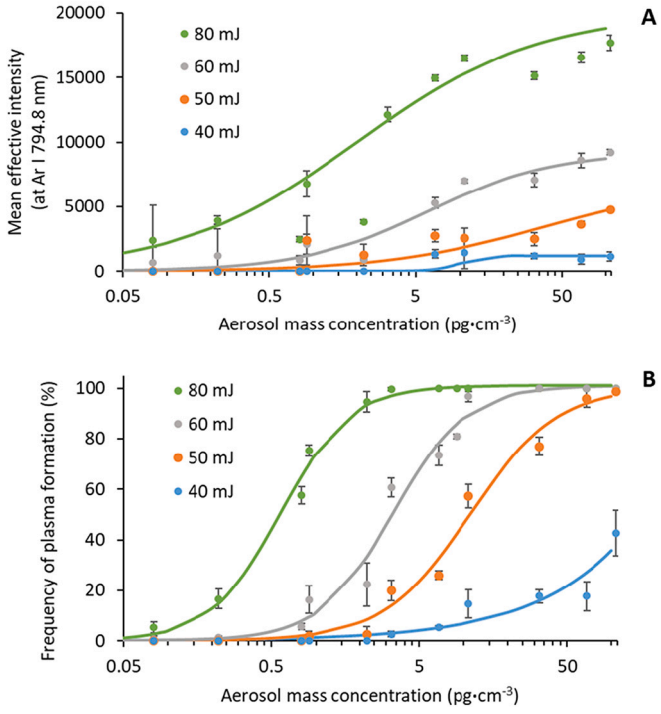

Fig. 6. The effect of the gold nanoaerosol mass concentration on the mean effective argon intensity (A) and the plasma formation frequency (B). Trendlines (cubic splines) are only meant to guide the eye. All values shown are based on the mean of three replicate measurements, each based on data from 100 laser shots. Errors bars indicate the standard deviation. (For interpretation of the references to colour in this figure legend, the reader is referred to the web version of this article.)

Fig. 6 shows the dependence of the plasma formation frequency and mean effective intensity on the aerosol mass concentration. The curves show a similar trend as in Fig. 4 (please note the logarithmic scale in Fig. 6). The plasma formation frequency increases with the mass concentration and reaches its maximum at a threshold concentration, the value of which is decreasing with the pulse energy. The presence of a 100% formation frequency plateau beyond a certain mass concentration is clearly discernible at 80 mJ pulse energy. The mean effective intensity curves also follow a similar pattern with a less pronounced asymptotic nature in the present concentration range.

The results shown in Fig. 6 can also be used to obtain the minimum laser pulse energy and/or aerosol mass concentration needed to produce argon plasmas under the present experimental conditions. The interrelation of the threshold pulse energy and aerosol mass concentration is illustrated in Fig. 7, where the thresholds were determined as the parameter values which gave rise to 50% plasma formation frequency (cf. Fig. 6 bottom). The threshold pulse energy asymptotically approaches a ca. 45 mJ value with the increase of the aerosol mass concentration, while the energy threshold corresponding to zero aerosol mass concentration would be around 100 mJ. Due to the exponentially decaying nature of the curve, this means that the laser breakdown threshold required for plasma formation can be decreased by a factor of ca. 2.2 by introducing as small as ca. 5 pg·cm^{-3} Au into the gas.

4. Discussion

According to the theory, the laser induced breakdown of materials (here: argon gas) is due to an electron avalanche (also called cascade) mechanism. The free electrons present or initially produced in the gas gain energy from the collisions with photons, with the participation of the particles of the gas (due to the momentum-energy conservation law) [3]. When some of the electrons acquire enough energy to ionize the gas particles, the electron concentration starts to grow and an electron avalanche is developed. The breakdown is somewhat arbitrarily defined

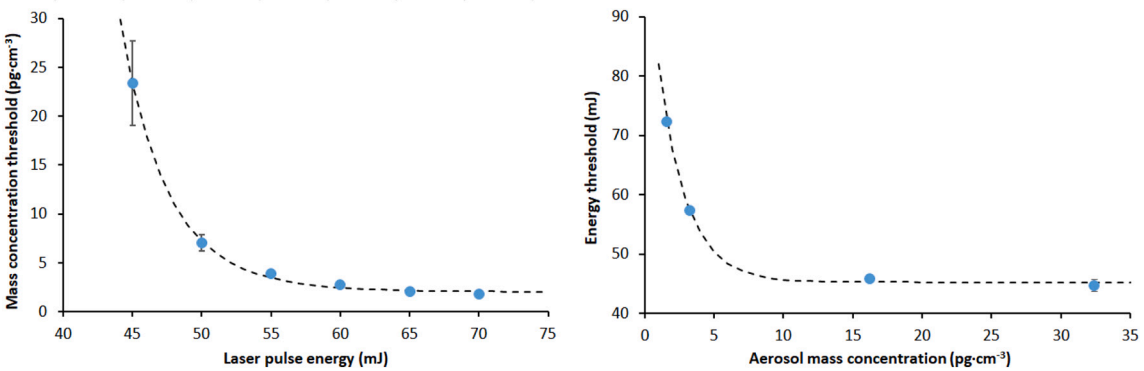

Fig. 7. The interrelation of the aerosol mass concentration and the laser pulse energy in terms of the breakdown threshold. Dashed trendlines are only meant to guide the eye. Errors bars indicate the standard deviation from three repeated measurements.

as the attainment of a certain electron concentration (e.g. 10^{15} cm^{-3}) or a small degree of ionization of the gas (e.g. 0.1%) sufficient to cause significant absorption and scattering of laser radiation, meaning that a "visible spark" (microplasma) is formed [35]. There is a minimum (threshold) breakdown power density (related to electrical field strength of the laser pulse) needed to generate the microplasma, which is determined by the balance between the electron concentration growth as well as the energy and electron losses due to inelastic collisions, stimulated radiation and recombination processes [3]. The combined duration of the initiation and growth steps is a couple of nanoseconds or less, that is also shorter than the duration of laser pulses typically used in LIBS [3,35]. For ultrapure, atmospheric pressure noble gases or air, the breakdown threshold irradiance is reported to be 10^{10}–10^{11} $W{\cdot}cm^{-2}$, which of course scales with the pressure of the gas, the laser pulse duration and laser focal spot diameter [35,36]. Bettis et al. have showed that the electrical field strength breakdown threshold can generally, for all solids, gases and liquids, be estimated with the formula

$$E_{th} \approx \frac{q_e \bullet \sqrt[3]{N^2}}{\varepsilon_0 \bullet (n^2 - 1)}$$

where q_e is the electron charge, N is the number density of atoms, ε_0 is the vacuum permittivity and n is the refractive index at the laser wavelength [36]. This calculation yields field strength values for atmospheric noble gases in good agreement with experimental values, if the pulse duration and focal spot diameter are also scaled to the experimental values from the theoretical 1 fs and 1 μm values. Scaling was found not to be necessary for wavelengths between 600 nm and 10 μm [36]. Threshold power density (irradiance, $W{\cdot}cm^{-2}$) values are proportional with the square of the field strength values.

The breakdown process therefore has to be initiated by the presence of free electrons (seed electrons) in the focal spot of the laser beam and a high enough laser power density. The source of the free electrons has been established in the literature to be either the ionization following the multiphoton absorption of the gas particles, or the result of the presence of impurities, Au NPs in our case. The presence of macro- and microscopic particles in gases has been found to considerably help the breakdown process, attributed to e.g. field amplification (forward focusing) or thermionic emission for particles with a diameter of tens of micrometers [2], but an increase in inverse bremsstrahlung rate caused by the explosion of particles has also been hypothesized [37].

In our case, at the 1064 nm laser wavelength and used photon fluxes the breakdown of the argon gas could not be observed in the absence of Au nanoparticles, implying that the prerequisites of multiphoton ionization of Ar are not met. However, in the presence of Au NPs, plasma formation clearly occurs (cf. Figs. 4-6) indicating that seed electrons are provided by the Au NPs. First of all, it should be mentioned that as opposed to the case of larger particles, having a diameter of tens of micrometers, [2], field amplification by forward focusing is negligible for nanoparticles, when the wavelength is much longer than the particle diameter. We would also like to emphasize that the effect is unlikely to be of plasmonic nature either. This is due to the fact that the very dilute, thus non-interacting nature of the relatively small Au NPs and the NIR excitation wavelength practically rules out the effective excitation of surface plasmons on the gold NPs or the field enhancement caused by their coupling, as opposed to situations examined in NP-enhanced LIBS studies [38,39].

Au NPs with a diameter in the 10–20 nm inefficiently absorb light at 1064 nm under conventional conditions, however, the relatively high laser intensity can compensate for this effect and electron temperatures sufficiently high for the thermionic effect can be quickly reached, thus electrons are able to eject from the particles. The fraction of such electrons may be as high as 0.001 at high enough laser intensities and/or absorption efficiencies [40]. It should also be noted that the peak absorbance of the Au NPs used in the present study happens to be centered just around 530 nm, therefore a two-photon laser light absorption might also be a viable process, considering that the absorption cross-section for Au NPs at this wavelength is about 5 orders of magnitude higher than that of conventional molecular dyes [41]. As a result, absorption of the laser light can lead to an efficient heating followed by thermoemission of electrons from the Au NPs even at the relatively low, ca. 10^6 cm^{-3} particle concentration.

In addition to this, field electron emission is also possible, since this process starts to become feasible for separated metallic nanoparticles above ca. 10^8 $V{\cdot}m^{-1}$ electrical field strength and the present laser parameters produce a value several times higher than. The work function for gold nanoparticles can be as low as 2.4 eV, significantly lower than for thin films [42,43]. These conditions make the photon-excited electron field emission from the Au NPs feasible. Furthermore, the number of free electrons produced separately by these processes scales with the volume of the NPs in the laser focal spot, and also increases with the laser pulse energy, which is in line with our observations (Fig. 5). The observation that the effect follows a nonlinear, asymptotically increasing function (Fig. 6) with the particle mass concentration can be explained by that the electron emission gives a positive charge to the particles, which works against electron emission. Thus, although the "total electron emission capacity" of a larger mass concentration aerosol is higher, but the equilibrium space charge will also set in sooner, which limits the magnitude of the effect.

As discussed above, the presence of gold NPs facilitates the plasma formation in argon via the two viable mechanisms described above, even at laser intensities insufficient for the breakdown of the pure gas. As shown in e.g. the top panel of Fig. 6 the higher is the particle mass concentration, the more intense is the Ar atomic emission signal. The excitation temperature of the plasma was also calculated using Ar I lines by using the Boltzmann plot method and Fig. 8 summarizes the variation of the temperature as a function of the aerosol mass concentration. The

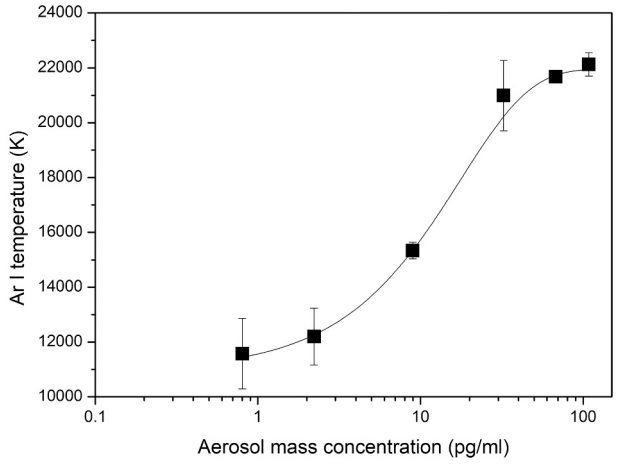

Fig. 8. Variation of the excitation temperature calculated from Ar I spectral lines as a function of the mass concentration of the Au nanoaerosol.

direct effect of the Au NPs on the Ar plasma temperature can be readily seen: a ca. two orders of magnitude increase in the particle mass concentration results in a ca. twofold increase in the Ar I temperature, following a trend closely resembling to those shown in Fig. 6.

Our observations above prove that not only various microparticles with tens of micrometer in diameter, e.g. "dust" [37], carbon, NaCl [1] or liquids [2,7] produce a significant decrease of the breakdown threshold, but also metallic nanoparticles. The finding that larger particles cause a larger effect also seems to hold for nanoparticles as well. The observed decrease in the breakdown threshold (with a factor of about 2.2, described with respect to Fig. 7) is relatively modest compared to the nearly two orders of magnitude reduction reported in the literature for the case of microparticles. Nevertheless, it is understandable considering that the particle volume, and hence the provided seed electrons for the breakdown is much lower for nanoparticles than microparticles, and that the contribution from forward-focusing is also missing. It shall also be added that the resulting enhancement in the (Ar) gas signal is at least 2–4 orders of magnitude, depending on the pulse energy (see Fig. 3 or Fig. 6)

It can also be mentioned that it seems to be quite safe to assume that the breakdown occurs outside the NPs in the argon gas. This assumption is facilitated by the fact that the number concentration of argon particles (atoms) is vastly higher than that of the gold NPs (ca. $2.5{\cdot}10^{19}$ cm^{-3} as opposed to 10^5–10^6 cm^{-3}, respectively). The microplasma, with a volume of about 10^{-3} cm^3 [44]) randomly forms within the focal spot of the laser beam in the argon gas and then expands and partially also breaks the NPs down. For the microplasma to be formed, the concentration of the NPs should be adequate in the focal spot volume to initiate the electron avalanche. This explains why the gold emission from the LIB plasma shows a very small (practically undetectable) intensity and why the argon emission intensity shows a great shot-to-shot variability. The polydisperse character of the Au NPs used also contributes to the fluctuation of the emission signal intensity.

Based on the above considerations, our experimental observations described in Sections 3.1 to 3.3. can be qualitatively explained (Fig. 9). Both the increase of the aerosol (mass) concentration and the laser pulse energy increases the number of seed electrons and hence the probability (frequency) of plasma formation, as well as the mean effective argon intensity.

5. Conclusions

It is worth pointing out that according to our observations, the plasma formation frequency is a function of the aerosol mass concentration, but the Au NPs are actually detected *indirectly*, via the influence of their presence on the breakdown of the carrier gas. Thus, the opportunity presents itself to use this effect for the determination of the mass concentration of a nanoaerosol in a range where the mass concentration is too small for the direct detection of NPs, after performing a calibration of the plasma formation frequency. The dynamic range of this indirect analysis is mainly limited by the mass concentration threshold (at lower pulse energies) and the frequency saturation (at high pulse energies). As it is suggested by the data presented in Fig. 6, it is possible to combine the calibration data in order to extend the dynamic range to 3.5–4 orders of magnitude (from ca. 0.05 $pg{\cdot}cm^{-3}$ to over 100 $pg{\cdot}cm^{-3}$); low mass concentrations can be determined by using high pulse energy (e.g. 80 mJ), whereas for high mass concentrations, low pulse energy (e.g. 50 mJ) should be used. Please note that the mean effective intensity of the argon line can also be used for the same indirect analysis following a similar calibration, with the potential that using a high dynamic range spectrometer (with an A/D resolution better than the 16 bit used in the present study), the signal saturation at around 100 $pg{\cdot}cm^{-3}$ can be avoided and an even wider mass concentration range may be accessed. It has to be noted though that this approach is only useful until the mass concentration at which the direct detection of the suspended nanoparticles also becomes possible [11,12,45].

We would also like to point out that from an analytical point of view, our observations also lead to an opportunity in trace gas analysis. A low mass concentration of gold NPs induces the aerosol carrier gas breakdown and therefore leads to the detection of gas plasma emission under conditions that would otherwise not be sufficient to achieve this. Although it is difficult to quantitate the gas signal enhancement in lack of a reference signal (there is no argon signal in the absence of NPs), but based on Figs. 4 and 6, it can be assumed to be in the 10^2 to 10^4 range. This presents the possibility to detect the gas particles with trace analytical sensitivity, while the emission spectrum is not complicated by the presence of peaks from the NPs. With the commercialization of compact SDGs, which was alluded to in the Introduction, it seems to be not impractical to conceptualize the use of an SDG to inject a gold

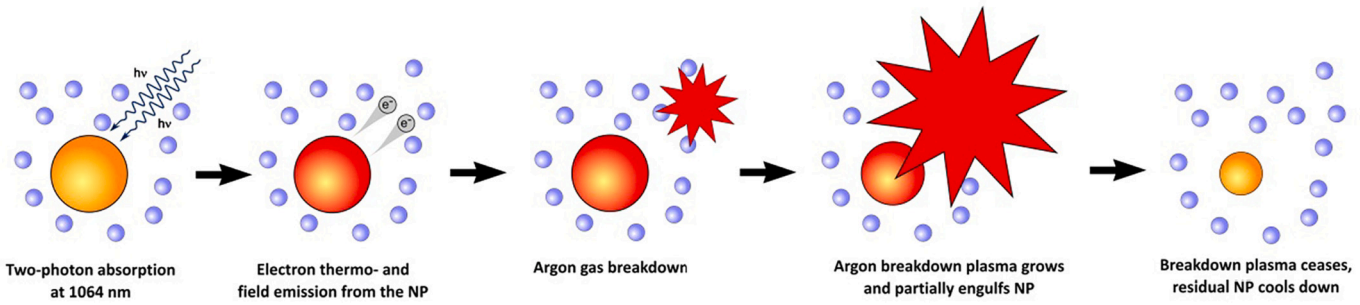

Fig. 9. Overview of the proposed processes occurring during laser induced breakdown of the gas in which nanoparticles are suspended (blue and orange spheres represent the gas particles and nanoparticles, respectively). (For interpretation of the references to colour in this figure legend, the reader is referred to the web version of this article.)

nanoaerosol into a stream of sample gas mixture (e.g. Ar mixed with other gases) for the purposes of gas analysis. The nanoaerosol carrier gas (e.g. N_2) would then become the major component in the gas mixture at a controlled mixing ratio, with the analyte gas present at a trace concentration. The concentration of the analyte gas in the original gas stream could be determined following a calibration of the analyte signal. The efficiency of Au NPs in producing seed electrons should also inhibit (cover) the breakdown threshold influencing, and therefore analyte signal calibration influencing, effect of any other particulate minor/trace contaminations present in the sample gas mixture. Experiments in the direction of demonstrating this analytical application are in progress in our laboratory.

In summary of our novel findings, it was found that the presence of gold NPs decreases the breakdown threshold of argon gas considerably, thereby facilitating the detection of Ar emission at such laser fluences, which do not allow plasma formation without the presence of the NPs. The effect was attributed to electron thermo- and field emission induced by the high intensity laser pulse. The argon signal shows an asymptotically increasing magnitude with the nanoaerosol mass concentration. We would like to emphasize that our observations were made at aerosol mass concentrations that are too low to allow the direct detection of nanoparticles. The observed effect is suggested to be useful in trace gas analysis or for the indirect detection of NPs. The achievable indirect aerosol mass concentration detection limit was estimated to be in the parts per trillion regime (as low as 50 $ng \cdot m^{-3}$) which is a value comparable to best literature values reported for direct analysis with much higher laser fluences or after preconcentration (e.g. [24,46,47].

CRediT authorship contribution statement

Dávid J. Palásti: Investigation, Data curation, Visualization, Writing – original draft. **Lajos P. Villy**: Investigation, Visualization. **Attila Kohut**: Validation, Visualization, Writing – review & editing. **Tibor Ajtai**: Conceptualization. **Zsolt Geretovszky**: Conceptualization. **Gábor Galbács**: Conceptualization, Funding acquisition, Supervision, Writing – review & editing.

Declaration of Competing Interest

There are no conflicts of interests to declare.

Acknowledgements

The authors gratefully acknowledge the financial support received from various sources including the National Research, Development and Innovation Office (through projects No. K 129063, PD 139077, EFOP-3.6.2-16-2017-00005, 2020-4.1.1.-TKP2020, TKP2021-NVA-19, New National Excellence Program 2021 and via the Nanoplasmonic Laser Fusion Research Laboratory NKFIH-468-3/2021) of Hungary.

References

[1] D.E. Lencioni, L.C. Pettingill, The dynamics of air breakdown initiated by a particle in a laser beam, J. Appl. Phys. 48 (1977), 1848–1581.
[2] P. Chýlek, M.A. Jarzembski, V. Srivastava, R.G. Pinnick, J.D. Pendleton, J. P. Cruncleton, Effect of spherical particles on laser-induced breakdown of gases, Appl. Opt. 26 (1987) 760–762.
[3] A.A. Lushnikov, A.E. Negin, Aerosols in strong laser beams, J. Aerosol Sci. 24 (1993) 707–735.
[4] B.W. Smith, D.W. Hahn, E. Gibb, I. Gornushkin, J.D. Winefordner, Laser induced plasma spectroscopy for the characterization of aerosols and particulates, KONA Powder Part J. 19 (2001) 25–33.
[5] Petr Chylek, Maurice A. Jarzembski, Vandana Srivastava, Ronald G. Pinnick, Pressure dependence of the laser-induced breakdown thresholds of gases and droplets, Appl. Opt. 29 (1990) 2303–2306.
[6] R.G. Pinnick, P. Chýlek, M. Jarzembski, E. Creegan, V. Srivastava, G. Fernandez, J. D. Pendleton, A. Biswas, Aerosol-induced laser breakdown thresholds: wavelength dependence, Appl. Opt. 27 (1988) 987–996.
[7] M.A. Petr Chýlek, N.Y. Jarzembski, R.G. Pinnick Chou, Effect of size and material of liquid spherical particles on laser-induced breakdown, Appl. Phys. Lett. 49 (1986) 1475–1477.
[8] A.P. Budnik, S.V. Zakharchenko, Optical breakdown in aerosols, Izv. AN SSSR, Set. Fizika 55 (1991) 1296–1304 (in Russian).
[9] Y. Raizer, Gas Discharge Physics, Springer, 2011.
[10] L.J. Radziemski, T.R. Loree, D.A. Cremers, N.M. Hoffman, Time-resolved laser-induced breakdown spectrometry of aerosols, Anal. Chem. 55 (1983) 1246–1252.
[11] D.W. Hahn, Laser-induced breakdown spectroscopy for analysis of aerosol particles: the path toward quantitative analysis, Spectroscopy 24 (2009) 26–33.
[12] H. Ji, Y. Ding, L. Zhang, Y. Hu, X. Zhong, Review of aerosol analysis by laser-induced breakdown spectroscopy, Appl. Spectrosc. Rev. 56 (2020) 193–220.
[13] U. Panne, D. Hahn, Analysis of aerosols by LIBS, Chapter 5, in: A.W. Miziolek, V. Palleschi, I. Schechter (Eds.), Laser Induced Breakdown Spectroscopy: Fundamentals and Applications, 2nd edition, Cambridge University Press, 2006.
[14] D. Hahn, U. Panne, LIBS for aerosol analysis, Chapter 17, in: J.P. Singh, S. N. Thakur (Eds.), Laser-Induced Breakdown Spectroscopy, *Elsevier*, 2007.
[15] D. Diaz, D.W. Hahn, Aerosol measurements with laser-induced breakdown spectroscopy and conditional analysis, Spectrochim. Acta B 179 (2021) 106107.
[16] T. Amodeo, C. Dutouquet, F. Tenegal, B. Guizard, H. Maskrot, O. Le Bihan, E. Frejafon, On-line monitoring of composite nanoparticles synthesized in a pre-industrial laser pyrolysis reactor using laser-induced breakdown spectroscopy, Spectrochim. Acta B 63 (2008) 1183–1190.
[17] T. Kuhlen, C. Fricke-Begemann, N. Strauss, R. Noll, Analysis of size-classified fine and ultrafine particulate matter on substrates with laser-induced breakdown spectroscopy, Spectrochim. Acta B 63 (2008) 1171–1176.
[18] P. Dewalle, J.-B. Sirven, A. Roynette, F. Gensdarmes, L. Golanski, S. Motellier, Airborne nanoparticle detection by sampling on filters and laser-induced breakdown spectroscopy analysis, J. Phys. Conf. Ser. 304 (2011), 012012.
[19] G. Galbács, A. Kéri, A. Kohut, M. Veres, Zs., Geretovszky: nanoparticles in analytical laser and plasma spectroscopy – a review of recent developments in methodology and applications, J. Anal. At. Spectrom. 36 (2021) 1826–1872.
[20] N. Strauss, C. Fricke-Begemann, R. Noll, Size-resolved analysis of fine and ultrafine particulate matter by laser-induced breakdown spectroscopy, J. Anal. At. Spectrom. 25 (2010) 867–874.
[21] F.J. Fortes, A. Fernández-Bravo, J.J. Laserna, Chemical characterization of single micro- and nano-particles by optical catapulting–optical trapping–laser-induced breakdown spectroscopy, Spectrochim. Acta B 100 (2014) 78–85.
[22] P. Purohit, F.J. Fortes, J.J. Laserna, Subfemtogram simultaneous elemental detection in multicomponent nanomatrices using laser-induced plasma emission spectroscopy within atmospheric pressure optical traps, Anal. Chem. 91 (2019) 7444–7449.
[23] Y. Zhang, G. Xiong, S. Li, Z. Dong, S.G. Buckley, S.D. Tse, Novel low-intensity phase-selective laser-induced breakdown spectroscopy of TiO_2 nanoparticle aerosols during flame synthesis, Combust. Flame 160 (2013) 725–733.
[24] P. Diwakar, P. Kulkarni, M.E. Birch, New approach for near-real time measurement of elemental composition of aerosol using laser-induced breakdown spectroscopy, Aerosol Sci. Technol. 46 (2012) 316–332.
[25] B.O. Meuller, M.E. Messing, D.L.J. Engberg, A.M. Jansson, L.I.M. Johansson, S. M. Norlén, N. Tureson, K. Deppert, Review of spark discharge generators for production of nanoparticle aerosols, Aerosol Sci. Technol. 46 (2012) 1256–1270.
[26] S. Bau, O. Witschger, F. Gensdarmes, D. Thomas, J.-P. Borra, Electrical properties of airborne nanoparticles produced by a commercial spark-discharge generator, J. Nanopart. Res. 12 (2010) 1989–1995.
[27] J. Lu, J. Guo, S. Song, G. Yu, H. Liu, X. Yang, Z. Lu, Preparation of Ag nanoparticles by spark ablation in gas as catalysts for electrocatalytic hydrogen production, RSC Adv. 10 (2020) 38583–38587.
[28] A. Schmidt-Ott (Ed.), Spark Ablation: Building Blocks for Nanotechnology, *Jenny Stanford Publishing*, 2020.
[29] A. Kohut, L. Ludvigsson, B.O. Meuller, K. Deppert, M.E. Messing, G. Galbács, Zs., Geretovszky: from plasma to nanoparticles: optical and particle emission of a spark discharge generator, Nanotechnology 28 (2017) 475603.
[30] A. Kohut, L.P. Villy, A. Kéri, Á. Bélteki, D. Megyeri, B. Hopp, G. Galbács, Zs., Geretovszky: full range tuning of the composition of Au/Ag binary nanoparticles by spark discharge generation, Sci. Rep. 11 (2021) 5117.
[31] A. Kohut, L.P. Villy, T. Ajtai, Zs. Geretovszky, G. Galbács, The effect of circuit resistance on the particle output of a spark discharge nanoparticle generator, J. Aerosol Sci. 118 (2018) 59–63.
[32] D.J. Palásti, A. Metzinger, T. Ajtai, Z. Bozóki, B. Hopp, É. Kovács-Széles, G. Galbács, Qualitative discrimination of coal aerosols by using the statistical evaluation of laser-induced breakdown spectroscopy data, Spectrochim. Acta B 153 (2019) 34–41.
[33] C. Aragón, J.A. Aguilera, Characterization of laser induced plasmas by optical emission spectroscopy: a review of experiments and methods, Spectrochim. Acta B 63 (2008) 893–916.
[34] A. Kramida, Yu. Ralchenko, J. Reader, NIST Atomic Spectra Database (ver. 5.9) [Online]. Available, https://physics.nist.gov/asd, National Institute of Standards and Technology, Gaithersburg, MD (USA), . February 9.
[35] F. Morgan, L.R. Evans, C.G. Morgan, Laser beam induced breakdown in helium and argon, J. Phys. D. Appl. Phys. 4 (1971) 225–235.
[36] J.R. Bettis, Correlation among the laser-induced breakdown thresholds in solids, liquids, and gases, Appl. Opt. 31 (1992) 3448–3452.
[37] D.E. Lencioni, The effect of dust on 10.6-μm laser-induced air breakdown, Appl. Phys. Lett. 23 (1973) 12–14.
[38] A. De Giacomo, M. Dell'Aglio, R. Gaudiuso, C. Koral, G. Valenza, Perspective on the use of nanoparticles to improve LIBS analytical performance: nanoparticle

enhanced laser induced breakdown spectroscopy (NELIBS), J. Anal. At. Spectrom. 31 (2016) 1566–1573.
[39] M. Dell'Aglio, R. Alrifai, A. De Giacomo, Nanoparticle enhanced laser-induced breakdown spectroscopy (NELIBS), a first review, Spectrochim. Acta B 148 (2018) 105–112.
[40] A. Pyatenko, M. Yamaguchi, M. Suzuki, Mechanisms of size reduction of colloidal silver and gold nanoparticles irradiated by Nd:YAG laser, J. Phys. Chem. C 21 (2009) 9078–9085.
[41] P.K. Jain, K.S. Lee, I.H. El-Sayed, M.A. El-Sayed, Calculated absorption and scattering properties of gold nanoparticles of different size, shape, and composition: applications in biological imaging and biomedicine, J. Phys. Chem. B 110 (2006) 7238–7248.
[42] S.A. Nepijko, H.J. Elmers, G. Schönhense, Emission properties of metal nanoparticles, Chapter 20, in: M. Aliofkhazraei (Ed.), Handbook of Nanoparticles, *Springer*, 2016.
[43] S. Dal Forno, L. Ranno, J. Lischner, Material, size, and environment dependence of plasmon-induced hot carriers in metallic nanoparticles, J. Phys. Chem. C 122 (2018) 8517–8527.
[44] J.E. Carranza, D.W. Hahn, Plasma volume considerations for analysis of gaseous and aerosol samples using laser-induced breakdown spectroscopy, J. Anal. At. Spectrom. 17 (2002) 1534–1539.
[45] G. Gallou, J.B. Sirven, C. Dutouquet, O. Le Bihan, E. Frejafon, Aerosols analysis by LIBS for monitoring of air pollution by industrial sources, Aerosol Sci. Technol. 45 (2011) 918–926.
[46] J.E. Carranza, B.T. Fisher, G.D. Yoder, D.W. Hahn, On-line analysis of ambient air aerosols using laser-induced breakdown spectroscopy, Spectrochim. Acta B 56 (2001) 851–864.
[47] D.W. Hahn, M.M. Lunden, Detection and analysis of aerosol particles by laser-induced breakdown spectroscopy, Aerosol Sci. Technol. 33 (2000) 30–48.